12th IFAC Symposium on Robot Control, Budapest, Hungary, August 27-30, 2018.
Paper No. 27.

# On the stability of two-wheeled vehicle balancing passive human subjects

**Balazs A. Kovacs** [*], **Gabor Stepan** [**], **Zaihua Wang** [***], **Tamas Insperger** [*]

[*] *Department of Applied Mechanics, Budapest University of Technology and Economics and MTA-BME Lendület Human Balancing Research Group, Budapest, Hungary, (e-mail: balazs.kovacs@mm.bme.hu, insperger@mm.bme.hu).*
[**] *Department of Applied Mechanics, Budapest University of Technology and Economics and MTA-BME Research Group on Dynamics of Machines and Vehicles, Budapest, Hungary, (e-mail: stepan@mm.bme.hu).*
[***] *State Key Laboratory of Mechanics and Control of Mechanical Structures, Nanjing University of Aeronautics and Astronautics, Nanjing, China, (e-mail: zhwang@nuaa.edu.cn).*

**Abstract:** A two-wheeled vehicle balancing a passive inverted pendulum is analyzed based on an experimental device. The corresponding mechanical model is a wheeled double pendulum, where only the position of the lower pendulum is measured. The sampling effect of the digital control is modeled as a zero-order hold. It is shown that the stabilization of the upright position is possible by proper choice of the control parameters as function of the sampling period of the controller. The model can be applied to analyze the behavior of wheeled vehicles with passive human subjects standing on it. The results are demonstrated on small-scale experimental realization of the system.

*Keywords:* wheeled inverted pendulum, stability, digital control

## 1. INTRODUCTION

Human balancing on moving vehicles is an actual topic nowadays. Standing still or walking while traveling on a train or an airplane is different from standing or walking on a sound floor. Perturbation coming from the moving floor and the visual perception of the moving environment can significantly effect the passengers' balancing abilities (Nesti et al., 2015). With the appearance of one or two-wheeled electric vehicles, new challenges have arisen (Segway, 2001; Nasrallah et al., 2007; Yang et al., 2013; Ye et al., 2016). Namely, the control mechanism of the vehicle should cooperate with the human subject driving the vehicle. The interaction of the human driver's reactions and the vehicle control mechanism results in a complex system with many uncertain parameters, mostly from the driver's side.

Unmanned versions of two-wheeled vehicles have been intensively analyzed, see, e.g, Zhou and Wang (2016); Kovacs and Insperger (2018). A main feature of the underlying control system is that it requires a feedback loop in order to compensate the perturbations originated from the environment. This inherently results in a dead time in the closed control loop, either analogue delay (Xu et al., 2017) or digital delay (Habib et al., 2017), which is typically considered to be a source of unstable behavior or poor performance. Experimental realization of simple balancing tasks is therefore not trivial (Gajamohan et al., 2013; Qin et al., 2014; Mühlebach and D´Andrea, 2017).

In case of human driven balancing vehicles, the feedback delay of the vehicle's control system interferes with the reaction time of the human subject, which often results in an undesired behavior and may even lead to fall. Human reaction delay for different tasks and the parameters of control mechanism employed by the human nervous system are typically unknown or can be estimated only with some uncertainty (Mehta and Schaal, 2002; Cabrera and Milton, 2004; Milton et al., 2016; Pasma et al., 2017; Zhang et al., 2018). Therefore the corresponding models involve uncertain parameters, which makes the evaluation of the results obtained using these models difficult. In this paper, a model is analyzed, where the control mechanism of the human subject is switched off. This gives a kind of transition between a vehicle driven by a human subject and an unmanned balancing vehicle. Namely, a human subject standing on a two-wheeled vehicle is modeled as an unstable inverted pendulum. The model is equivalent to a wheeled double inverted pendulum.

## 2. MECHANICAL MODEL

An experimental two-wheeled balancing unit shown in Fig. 1 was used as a basis of the mechanical model. The cart is controlled by a micro-controller of type STM32F103C8T6. The position of the cart is measured by a 3-axis acceleration and gyro sensor. The sampling frequency of the accelerometer is 1 kHz. The sampling frequency of the gyro is 8 kHz.

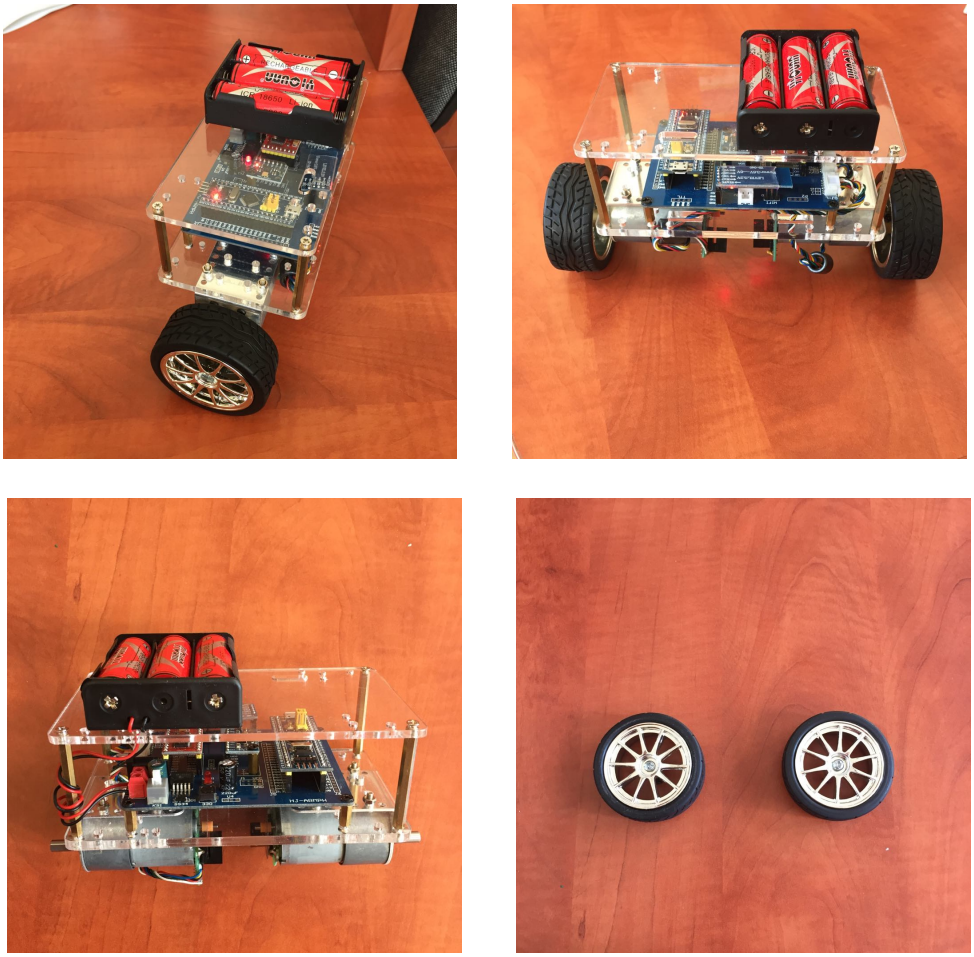

Fig. 1. Experimental wheeled balancing device (top) and the body of the cart wheels (bottom).

The mechanical model of the system is shown in Fig. 2. The system has three degrees of freedom. The corresponding generalized coordinates are chosen to be the angular position $\vartheta$ of the wheel, the angular position $\psi$ of the body of the vehicle (cart) and the angular position $\varphi$ of the pendulum. The pendulum models a human subject standing on the cart without any active control. The torsional stiffness $s_\mathrm{t}$ and damping $k_\mathrm{t}$ model the passive stiffness and damping of the human ankle. According to Loram and Lakie (2002), this stiffness is not enough to stabilize the upper equilibrium and, during standing still, an active control is required at the ankles for stabilization. In this model, we assume that the active control is switched off and the subject is standing still passively and we rely on the control of the cart to stabilize the human (together with the cart). Following Loram and Lakie (2002), the stiffness was estimated to be about 91% of the critical stiffness that is necessary to provide minimal stabilization, which gives $s_\mathrm{t} = 0.91 m_\mathrm{s} g l_{pS2} = 0.0446$ Nm/rad. The passive damping coefficient is chosen to be $k_\mathrm{t} = 1.531 \times 10^4$ Nms/rad, which gives the same damping ratio of 0.08924 as in Asai et al. (2009).

The geometry and the inertial parameters of the wheeled cart has been determined by measuring the elements of the experimental device (see Fig. 1 and Table 1). The parameters of the inverted pendulum are given in Table 2.

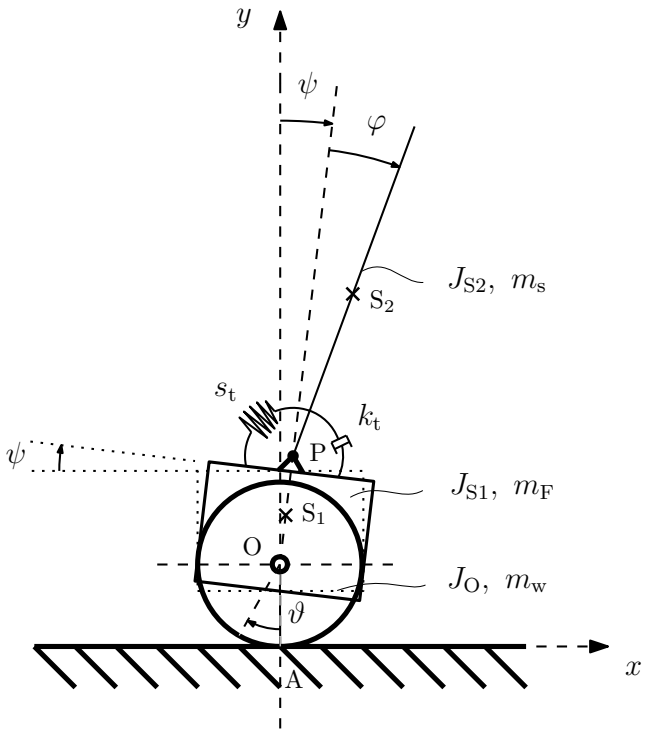


Fig. 2. The mechanical model of the passive segway–human interaction.

Table 1. Parameters of the wheeled cart.

| Measured property | Value | Description |
|---|---|---|
| $R$ | 0.032 m | radius of the wheel |
| $l_{\mathrm{OS1}}$ | 0.031 m | distance between the axis of the wheel and the center of mass of the cart |
| $l_{\mathrm{OP}}$ | 0.08 m | distance between the axis of the wheel and the pivot point P of the pendulum |
| $m_{\mathrm{w}}$ | 0.0467 kg | mass of the wheels |
| $m_{\mathrm{F}}$ | 0.7474 kg | mass of the cart frame |
| $J_{\mathrm{O}}$ | $3.66\times10^{-5}$ kgm$^2$ | mass moment of inertia of the wheel wrt the normal axis of the plane through point O |
| $J_{\mathrm{F}}$ | $87.7\times10^{-5}$ kgm$^2$ | mass moment of inertia of the frame wrt the normal axis of the plane through point $S_1$ |

Table 2. Parameters of the passive inverted pendulum.

| Properties of the stick | Value | Description |
|---|---|---|
| $l_{\mathrm{PS2}}$ | 0.1 m | distance of the center of mass of the stick from the pivot point P |
| $m_{\mathrm{s}}$ | 0.05 kg | mass of the stick |
| $J_{\mathrm{S2}}=\frac{1}{3}m_{\mathrm{s}}l_{\mathrm{PS2}}^2$ | $16.667\times10^{-5}$ kgm$^2$ | mass moment of inertia of the stick wrt the normal axis of the plane through point $S_2$ |

The system is governed by the differential equation

$$\begin{bmatrix} M_{11} & M_{12} & M_{13} \\ M_{21} & M_{22} & M_{23} \\ M_{31} & M_{32} & M_{33} \end{bmatrix} \begin{bmatrix} \ddot{\vartheta} \\ \ddot{\psi} \\ \ddot{\varphi} \end{bmatrix} + \begin{bmatrix} f_1(\varphi,\dot{\varphi},\psi,\dot{\psi}) \\ f_2(\varphi,\dot{\varphi},\psi,\dot{\psi}) \\ f_2(\varphi,\dot{\varphi},\psi,\dot{\psi}) \end{bmatrix} = \begin{bmatrix} 1 \\ -1 \\ 0 \end{bmatrix} Q, \quad (1)$$

where

$$\begin{aligned}
M_{11} =& (m_{\mathrm{s}}+m_{\mathrm{F}}+m_{\mathrm{w}})R^2+J_{\mathrm{O}},\\
M_{12} =& R((l_{\mathrm{OP}}m_{\mathrm{s}}+l_{\mathrm{OS1}}m_{\mathrm{F}})\cos(\psi)+l_{\mathrm{PS2}}m_{\mathrm{s}}\cos(\varphi+\psi)),\\
M_{13} =& l_{\mathrm{PS2}}m_{\mathrm{s}}R\cos(\varphi+\psi),\\
M_{21} =& R((l_{\mathrm{OP}}m_{\mathrm{s}}+l_{\mathrm{OS1}}m_{\mathrm{F}})\cos(\psi)+l_{\mathrm{PS2}}m_{\mathrm{s}}\cos(\varphi+\psi)),\\
M_{22} =& m_{\mathrm{F}}l_{\mathrm{OS1}}^2+J_{\mathrm{S2}}+J_{\mathrm{S1}}+\left(l_{\mathrm{OP}}^2+l_{\mathrm{PS2}}^2\right)m_{\mathrm{s}}\\
&+2l_{\mathrm{OP}}l_{\mathrm{PS2}}m_{\mathrm{s}}\cos(\varphi),\\
M_{23} =& m_{\mathrm{s}}(l_{\mathrm{PS2}}^2+l_{\mathrm{OP}}l_{\mathrm{PS2}}\cos(\varphi))+J_{\mathrm{S2}},\\
M_{31} =& l_{\mathrm{PS2}}m_{\mathrm{s}}R\cos(\varphi+\psi),\\
M_{32} =& m_{\mathrm{s}}(l_{\mathrm{PS2}}^2+l_{\mathrm{OP}}l_{\mathrm{PS2}}\cos(\varphi))+J_{\mathrm{S2}},\\
M_{33} =& m_{\mathrm{s}}l_{\mathrm{PS2}}^2+J_{\mathrm{S2}}
\end{aligned}$$

$$\begin{aligned}
f_1(\varphi,\dot{\varphi},\psi,\dot{\psi}) =& -R\dot{\psi}^2\sin(\psi)(l_{\mathrm{OP}}m_{\mathrm{s}}+l_{\mathrm{OS1}}m_{\mathrm{F}})\\
&+Rl_{\mathrm{PS2}}m_{\mathrm{s}}(\dot{\varphi}+\dot{\psi})^2\sin(\varphi+\psi),\\
f_2(\varphi,\dot{\varphi},\psi,\dot{\psi}) =& -g(\sin(\psi)(l_{\mathrm{OP}}m_{\mathrm{s}}+l_{\mathrm{OS1}}m_{\mathrm{F}})\\
&+l_{\mathrm{PS2}}m_{\mathrm{s}}\sin(\varphi+\psi))\\
&-l_{\mathrm{OP}}l_{\mathrm{PS2}}m_{\mathrm{s}}\dot{\varphi}\sin(\varphi)(\dot{\varphi}+2\dot{\psi}),\\
f_2(\varphi,\dot{\varphi},\psi,\dot{\psi}) =& -gl_{\mathrm{PS2}}m_{\mathrm{s}}\sin(\varphi+\psi)\\
&+l_{\mathrm{OP}}l_{\mathrm{PS2}}m_{\mathrm{s}}\dot{\psi}^2\sin(\varphi)+s_{\mathrm{t}}\varphi+k_{\mathrm{t}}\dot{\varphi},
\end{aligned}$$

The control torque acting between the wheels and the cart is assumed in the form

$$Q=P_\vartheta\vartheta+D_\vartheta\dot{\vartheta}+P_\psi\psi+D_\psi\dot{\psi}, \quad (2)$$

where $P_\vartheta$, $D_\vartheta$, $P_\psi$ and $D_\psi$ are the control gains. Note that the angle $\varphi$ and its derivative $\dot{\varphi}$ do not show up in the control law.

In order to analyze stability properties about the upper equilibrium, the system should be linearized. The linearized equation of motion has the form

$$\mathbf{M}\ddot{\mathbf{q}}(t)+\mathbf{D}\dot{\mathbf{q}}(t)+\mathbf{S}\mathbf{q}(t)=\mathbf{H}u(t), \quad (3)$$

$$u(t)=\mathbf{K}_{\mathrm{p}}^{\mathrm{T}}\mathbf{q}(t_i)+\mathbf{K}_{\mathrm{d}}^{\mathrm{T}}\dot{\mathbf{q}}(t_i), \quad t\in[t_i,t_{i+1}) \quad (4)$$

where $t_i=i\Delta t$ are the sampling instants with $\Delta t$ being the sampling period of the digital controller. Here, $\mathbf{M}$ is the same as the mass matrix in (1) with setting all the cos functions to 1,

$$\mathbf{S}=\begin{bmatrix} 0 & 0 & 0 \\ 0 & -gl_{\mathrm{PS2}}m_{\mathrm{s}}-g(l_{\mathrm{OP}}m_{\mathrm{s}}+l_{\mathrm{OS1}}m_{\mathrm{F}}) & -gl_{\mathrm{PS2}}m_{\mathrm{s}} \\ 0 & -gl_{\mathrm{PS2}}m_{\mathrm{s}} & s_{\mathrm{t}}-gl_{\mathrm{PS2}}m_{\mathrm{s}} \end{bmatrix},$$

$$\mathbf{D}=\begin{bmatrix} 0 & 0 & 0 \\ 0 & 0 & 0 \\ 0 & 0 & k_{\mathrm{t}} \end{bmatrix}, \quad \mathbf{H}=\begin{bmatrix} 1 \\ -1 \\ 0 \end{bmatrix}$$

are the stiffness, the damping and the input matrices, respectively, $u$ is the control input and

$$\mathbf{K}_{\mathrm{p}}=\begin{bmatrix} P_\vartheta \\ P_\psi \\ 0 \end{bmatrix}, \quad \mathbf{K}_{\mathrm{d}}=\begin{bmatrix} D_\vartheta \\ D_\psi \\ 0 \end{bmatrix}$$

are the vectors of the control gains.

## 3. STABILITY ANALYSIS AND NUMERICAL SIMULATIONS

First-order representation of the system reads

$$\dot{\mathbf{x}}(t)=\mathbf{A}\mathbf{x}(t)+\mathbf{B}u(t), \quad (5)$$

$$u(t)=\mathbf{K}^T\mathbf{x}(t_i), \quad t\in[t_i,t_{i+1}) \quad (6)$$

where

$$\mathbf{A}=\begin{bmatrix} \mathbf{0}_{3\times3} & \mathbf{I}_{3\times3} \\ -\mathbf{M}^{-1}\mathbf{S} & -\mathbf{M}^{-1}\mathbf{D} \end{bmatrix},$$

$$\mathbf{B}=\begin{bmatrix} \mathbf{0}_{3\times1} \\ \mathbf{M}^{-1}\mathbf{H} \end{bmatrix}, \qquad \mathbf{K}=\begin{bmatrix} \mathbf{K}_{\mathrm{p}} \\ \mathbf{K}_{\mathrm{d}} \end{bmatrix}$$

Here $\mathbf{0}_{3\times3}$ and $\mathbf{I}_{3\times3}$ stands for the zero and identity matrices of size $3\times3$. Solving this system over a sampling period of the controller gives the discrete map of the form

$$\mathbf{z}_{i+1}=\mathbf{G}\mathbf{z}_i \quad (7)$$

where

$$\mathbf{G}=\begin{bmatrix} \mathbf{P} & \mathbf{R} \\ \mathbf{K}^T & 0 \end{bmatrix} \quad (8)$$

is the state-transition matrix and

$$\mathbf{P}=\mathrm{e}^{\mathbf{A}\Delta t}, \qquad \mathbf{R}=\int_0^{\Delta t}\mathrm{e}^{\mathbf{A}(\Delta t-s)}\mathrm{d}s\mathbf{B}. \quad (9)$$

Stability of the upright position is determined by the eigenvalues of matrix $\mathbf{G}$. If all the eigenvalues are in modulus less than one, then the system is stable.

Stability properties in the 4-dimensional space of the control gains $P_\vartheta$, $D_\vartheta$, $P_\psi$ and $D_\psi$ are illustrated by a set of stability diagrams in the plane $(P_\psi, D_\psi)$ for fixed

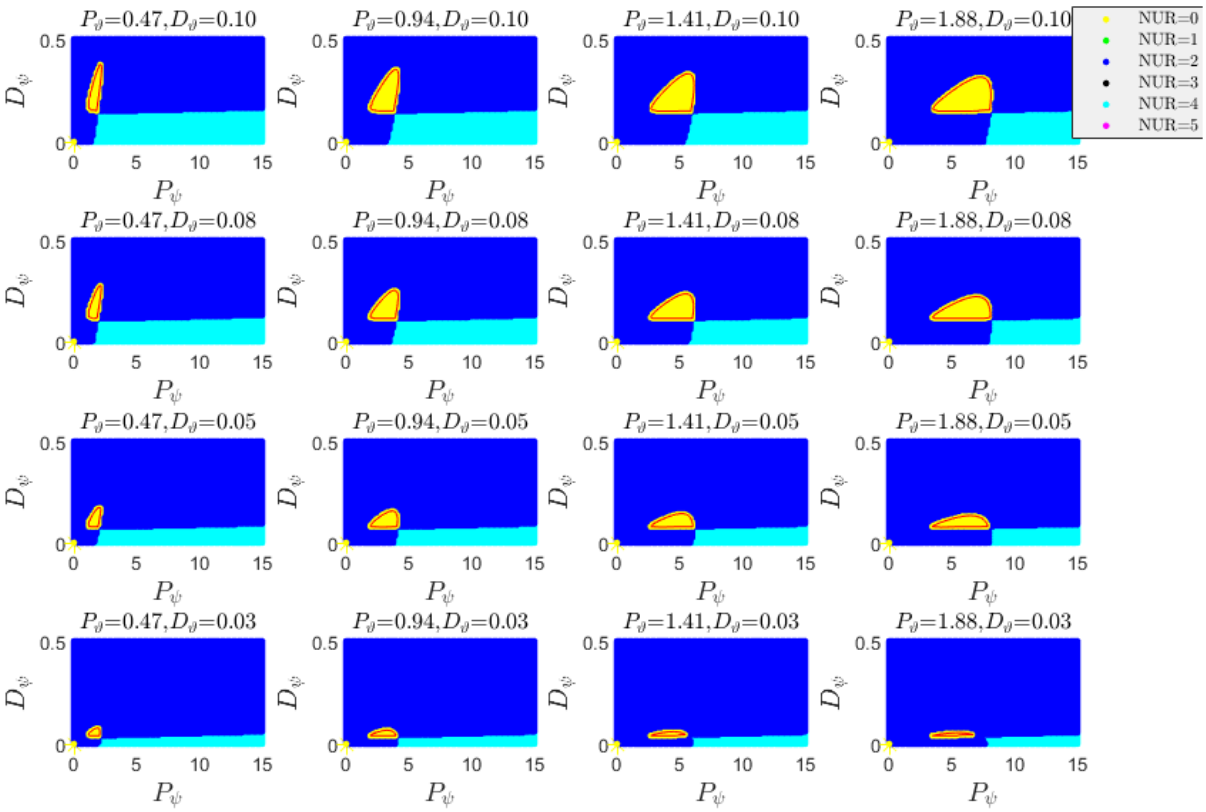


Fig. 3. Stability diagrams in the 4D parameter space. The colored spots represent the number of unstable roots (NUR). The system is stable if NUR=0.

pairs of $(P_\vartheta, D_\vartheta)$ as shown in Fig. 3. The eigenvalues of the system was evaluated at a $100 \times 100$ grid of the plain $(P_\vartheta, D_\vartheta)$. Different colors indicate the number of unstable roots (NUR), i.e., the number of eigenvalues of matrix $\mathbf{G}$ whose magnitude are larger than one. Stabilizing control gains are associated with yellow color (NUR= 0). Dark blue and light blue colors indicates NUR= 2 and 4. This indicates that along the transition curves between the yellow and the dark blue and between the dark and the light blue regions, a complex pair of eigenvalues crosses the unit circle of the complex plane. Thus, the system becomes unstable in an oscillatory way.

Time domain simulation associated with a set of stabilizing control gains is shown in Fig. 4 with a reasonable damping value. This demonstrates that the system can be stabilized even if the angle $\varphi$ of the human subject is not measured. If the damping in the system is small or zero, then asymptotic stabilization is not possible, since the smallest perturbations originated from the initial conditions result in an undamped oscillation.

## 4. EXPERIMENTAL RESULTS

A conventional PID control was used, which requires the measurement of the angular positions and the angular velocities of the wheel and the cart's body. In order to validate the model, some measurements were made with the device. A motion capture system was used to record the motion of the self-balancing vehicle. Three markers were placed on the body of the cart, which allowed the calculation of the angular position of the body of the cart. Two measurements were made.

First, the cart was left alone to balance itself and no perturbation was applied. The resulted motion of the cart can be seen in Fig. 5. The oscillatory nature of the recorded motion indicates the possibility of the existence of limit cycles, which might be the result of unmodelled nonlinear effects, such as sensory dead zones or actuation quantization. On the other hand, the motion is not purely periodic, which indicates either noise or chaotic behavior. In order to indicate chaotic motions, the maximal Lyapunov exponent was calculated using Wolf's method (Wolf et al., 1985), which gave a slightly positive value: $\lambda_{\max} = 0.1292$. Thus, chaos is also an essential component of the motion of the computer controlled device.

Second, perturbation tests were performed in order to determine the control gain parameters. A series of simulation were carried out for $8^4$ different parameter combinations of $(P_\vartheta, D_\vartheta, P_\psi, D_\psi)$ and the maximum norm of the error $\varepsilon(t) = \psi_{\text{meas.}}(t) - \psi_{\text{sim.}}(t)$ was chosen to measure the quality of the fitted solution. The control gain parameters that were calculated are the following: $P_\vartheta = 1.875$, $D_\vartheta = 0.1$, $P_\psi = 18.75$, $D_\psi = 0.25$. The result is shown in Fig. 6.

## 5. CONCLUSION

The presented mechanical model of the self-balancing vehicle compared to the experimental device has many simplifications. The effect of friction in the drive and the electro-mechanical behavior of the system are neglected.

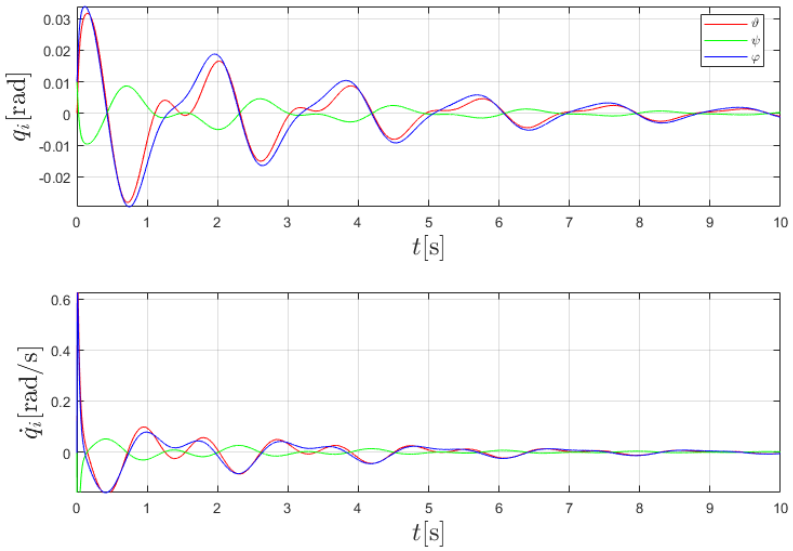


Fig. 4. Simulations for the control parameters $P_\theta = 1.875$, $D_\theta = 0.1$, $P_\psi = 6.25$ and $D_\psi = 0.25$ with damping coefficient $k_\mathrm{t} = 1.531 \times 10^4$ Nms/rad.

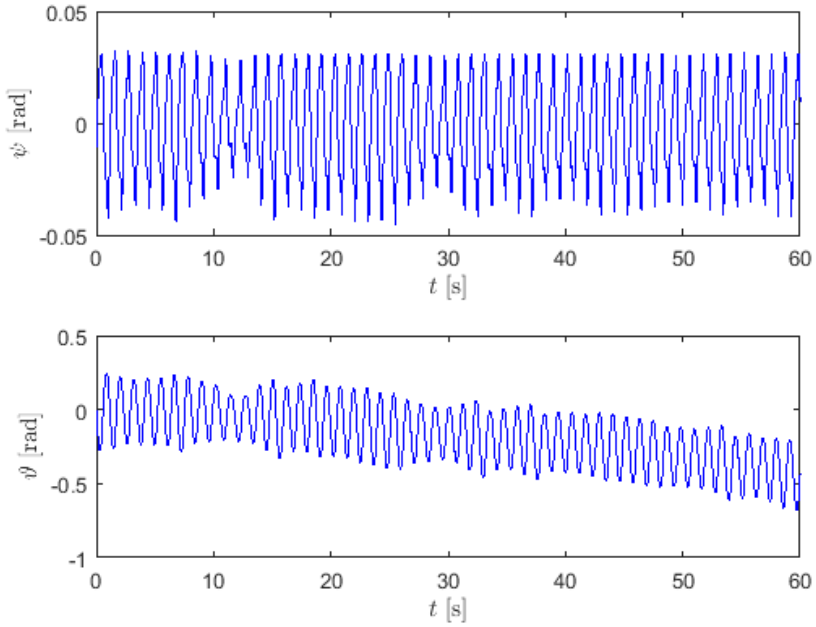


Fig. 5. Periodic motions of the cart.

Also, motor saturation and the dead zones of the sensors were not modeled. Although these effect do not typically affect global behavior, locally they may result in bounded oscillations or even chaotic motions. Chaotic oscillations in digitally controlled machines is a consequence of spatial quantization and temporal sampling of the controller. Because the amplitude of the resulted oscillations often scaled to the quantization step and is therefore small, this phenomenon is called micro chaos (Haller and Stépán, 1996).

Considering the parameters and results of the simplified mechanical model, the proposed task, namely the passive human standing on the self-balancing vehicle, can be achieved with proper control gain parameters. The simulation shows that the passive damping of the human ankle plays a significant role in the stability. Without the damping, the system is only marginally stable (it has a pair of pure imaginary eigenvalues).

## ACKNOWLEDGEMENTS

This work was supported by the Hungarian National Development Agency under grant number TET-12-CN-1- 2012-0012. The research leading to these results has received funding partially from the European Research Council under the European Union's Seventh Framework Programme (FP/2007-2013)/ERC Advanced grant agreement no.340889. The research reported in this paper was

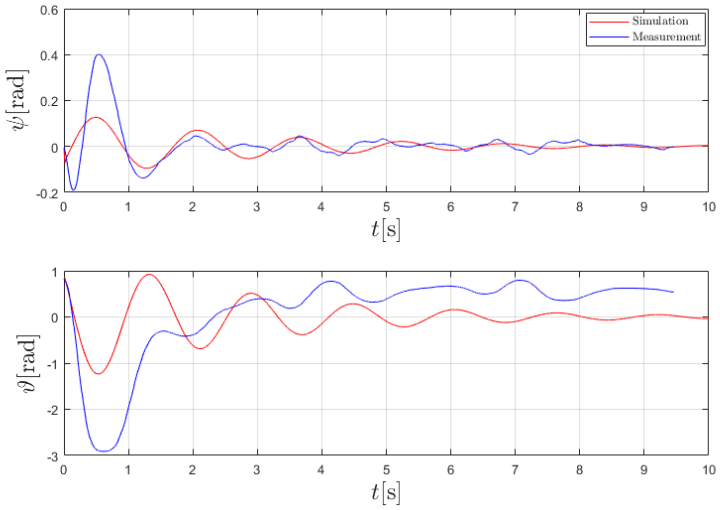


Fig. 6. The comparison of the measured and the simulated motion with fitted PD parameters.

supported by the Higher Education Excellence Program of the Ministry of Human Capacities in the frame of Artificial intelligence research area of Budapest University of Technology and Economics (BME FIKP-MI).

## REFERENCES

Asai, Y., Tasaka, Y., Nomura, K., Nomura, T., Casadio, M., and Morasso, P. (2009). A model of postural control in quiet standing: Robust compensation of delay-induced instability using intermittent activation of feedback control. *PLOS ONE*, 4(7), 1–14.

Cabrera, J.L. and Milton, J.G. (2004). Human stick balancing: Tuning lèvy flights to improve balance control. *Chaos*, 14, 691–698.

Gajamohan, M., Muehlebach, M., Widmer, T., and D´Andrea, R. (2013). The Cubli: a reaction wheel based 3D inverted pendulum. In *European Control Conference (ECC)*, 268.

Habib, G., Miklos, A., Enikov, E. T. an Stepan, G., and Rega, G. (2017). Nonlinear model-based parameter estimation and stability analysis of an aeropendulum subject to digital delayed control. *International Journal of Dynamics and Control*, 5(3), 629–643.

Haller, G. and Stépán, G. (1996). Micro-chaos in digital control. *Journal of Nonlinear Science*, 6(5), 415–448.

Kovacs, B.A. and Insperger, T. (2018). Retarded, neutral and advanced differential equation models for balancing using an accelerometer. *International Journal of Dynamics and Control*, 6(2), 694–706.

Loram, I. and Lakie, M. (2002). Direct measurement of human ankle stiffness during quiet standing: the intrinsic mechanical stiffness is insufficient for stability. *The Journal of Physiology*, 545, 1041–1053.

Mehta, B. and Schaal, S. (2002). Forward models in visuomotor control. *Journal of Neurophysiology*, 88, 942–953.

Milton, J., Meyer, R., Zhvanetsky, M., Ridge, S., and Insperger, T. (2016). Control at stabilitys edge minimizes energetic costs: expert stick balancing. *Journal of the Royal Society Interface*, 13, 20160212.

Mühlebach, M. and D´Andrea, R. (2017). Nonlinear analysis and control of a reaction-wheel-based 3-D inverted pendulum. *IEEE Transactions on Control Systems Technology*, 25(1), 235–246.

Nasrallah, D.S., Michalska, H., and Angeles, J. (2007). Controllability and posture control of a wheeled pendulum moving on an inclined plane. *IEEE Transactions on Robotics*, 23(3), 564–577.

Nesti, A., Beykirch, K.A., Pretto, P., and Bülthoff, H.H. (2015). Self-motion sensitivity to visual yaw rotations in humans. *Experimental Brain Research*, 233(3), 861–869.

Pasma, J.H., Boonstra, T.A., van Kordelaar, J., Spyropoulou, V.V., and Schouten, A.C. (2017). A sensitivity analysis of an inverted pendulum balance control model. *Frontiers in Computational Neuroscience*, 11, 99.

Qin, Z.C., X., L., Zhong, S., and Sun, J.Q. (2014). Control experiments on time-delayed dynamical systems. *Journal of Vibration and Control*, 20(6), 827–837.

Segway (2001). *Available at: http://www.segway.com/*, (accessed 9 March 2018).

Wolf, A., Swift, J.B., Swinney, H.L., and Vastano, J.A. (1985). Determining lyapunov exponents from a time series. *Physica D: Nonlinear Phenomena*, 16(3), 285–317.

Xu, Q., Stepan, G., and Wang, Z. (2017). Balancing a wheeled inverted pendulum with a single accelerometer in the presence of time delay. *Journal of Vibration and Control*, 23(4), 604–614.

Yang, C., Li, Z., and Li, J. (2013). Trajectory planning and optimized adaptive control for a class of wheeled inverted pendulum vehicle models. *IEEE Transactions on Cybernetics*, 43(1), 24–36.

Ye, W., Li, Z., Yang, C., Sun, J., Su, C.Y., and Lu, R. (2016). Vision-based human tracking control of a wheeled inverted pendulum robot. *IEEE Transactions on Cybernetics*, 46(11), 2423–2434.

Zhang, L., Stepan, G., and Insperger, T. (2018). Saturation limits the contribution of acceleration feedback to balancing against reaction delay. *Journal of the Royal Society Interface*, 15, 20170771.

Zhou, Y. and Wang, Z. (2016). Robust motion control of a two-wheeled inverted pendulum with an input delay based on optimal integral sliding mode manifold. *Nonlinear Dynamics*, 85(3), 2065–2074.